Theory of Ferromagnetic Resonance Line Shape outside the Spin-Wave Manifold*

K. MOTIZUKI† AND M. SPARKS‡
Microwave Laboratory, W. W. Hansen Laboratories of Physics, Stanford University, Stanford, California

AND

P. E. SEIDEN
IBM Watson Research Center, Yorktown Heights, New York

(Received 4 June 1965)

In the usual ferromagnetic resonance experiment the uniform precession lies within the magnon manifold, that is, there are long-wavelength magnons degenerate with the uniform precession. Several recent experiments have been performed with the uniform precession driven outside the magnon manifold. In this paper we calculate the line shape (χ'' as a function of applied field) for these experiments. Specifically, the relaxation frequency η of the uniform precession and the line shift δH (deviation of the uniform precession frequency from the Kittel frequency) are calculated. For relatively large η ($\eta \ll \gamma 4\pi M$ not satisfied) the line shift δH is at least as important as η in determining the line shape. Explanations are given for the three interesting observations of Liu and Shaw that: (1) The relaxation frequency has the large value of the order of 150 Oe when the uniform precession is driven below the bottom of the spin-wave manifold; (2) The relaxation frequency drops sharply as the uniform precession passes below the bottom of the spin-wave manifold; and (3) The relaxation frequency within the spin-wave manifold is relatively independent of applied field. Examination of several possible sources of the 150-Oe relaxation frequency (1) indicates that the 150 Oe arises from the magnon manifold being modified by nonmagnetic voids in the sample in such a way as to allow two-magnon scattering below the magnon manifold of a perfectly dense sample. The field independence of relaxation frequency within the manifold (2) is in apparent agreement with the two-magnon scattering theory of Sparks, Loudon, and Kittel; Seiden; and Seiden and Sparks.

I. INTRODUCTION

In several recent ferromagnetic-resonance experiments[1–4] the uniform precession (or other magnetostatic modes[5,6]) was excited outside the magnon manifold. When the linewidths were large inside the manifold, it was found[1–4] that the linewidth was also relatively large outside the manifold. The linewidth and line shape are determined[7] by the relaxation frequency η and line shift δH of the uniform precession. In the present paper the relaxation frequency and line shift of the uniform precession are calculated and discussed.

In the paper by Liu and Shaw,[1] hereafter referred to as I, the imaginary part of the susceptibility χ'' of a disk-shaped sample of yttrium iron garnet is measured both below and above the bottom of the bulk magnon manifold, that is, the manifold appropriate to the perfectly dense sample. In Sec. II we shall see that nonmagnetic inclusions in the sample modify the manifold. For the uniform precession above the bottom of the bulk manifold, the relaxation frequency has a value of 650 Oe (strictly speaking, a relaxation frequency corresponding to a full linewidth of 650 Oe), and for the uniform precession below the bottom of the bulk manifold the relaxation frequency is of the order of 150 Oe. The purposes of this paper are to present an explanation of the relatively large value (150 Oe in I) of line width remaining when the uniform precession is outside the bulk manifold and a discussion of the field dependence of the relaxation frequency within the bulk manifold.

In the usual linewidth experiments in ferromagnetic insulators the applied rf field excites the uniform precession spin-wave mode. An important and often dominant source of line width is the two-magnon process, in which a uniform precession magnon is annihilated and a magnon of nonzero wave vector having the same energy as the uniform-precession magnon is created. This two-magnon process can be induced by pits left on the surface by the sample polishing process,[8–12] voids and nonmagnetic inclusions in the sample,[8–12] polycrystalline grains,[13] or ion-to-ion disorder.[14,15] The

* The portion of the research conducted at Stanford University was supported jointly by the National Science Foundation and the Advanced Research Projects Agency through the Center for Materials Research at Stanford University.

† Present Address: Department of Physics, Osaka University, Toyonaka, Osaka, Japan.

‡ Alfred P. Sloan Research Fellow.

[1] S. G. Liu and H. J. Shaw (to be published); S. G. Liu, Stanford University Microwave Laboratory, Report No. 1092, 1963 (unpublished).

[2] A. Risley and H. Bussey, J. Appl. Phys. **35**, 896 (1964).

[3] A. Risley and H. Bussey (private communication).

[4] C. R. Buffler, J. Appl. Phys. **30**, 172S (1959); **31**, 222S (1960).

[5] R. L. White, J. Appl. Phys. **30**, 182S (1959).

[6] J. Nemarich, Phys. Rev. **136**, A1657 (1964).

[7] M. Sparks (to be published). Line shifts δH are calculated and the importance of δH in determining line shape are discussed.

[8] R. C. LeCraw, E. G. Spencer, and C. S. Porter, Phys. Rev. **110**, 1311 (1958).

[9] A. G. Gurevich and I. E. Gubler, Fiz. Tverd. Tela **1**, 1847 (1959) [English transl.: Soviet Phys.—Solid State **1**, 1693 (1960)].

[10] M. Sparks, R. Loudon, and C. Kittel, Phys. Rev. **127**, 791 (1961).

[11] P. Seiden and M. Sparks, Phys. Rev. **137**, A1278 (1965).

[12] M. Sparks, *Ferromagnetic Relaxation Theory* (McGraw-Hill Book Company, Inc., New York, 1964).

[13] P. E. Seiden and J. G. Grunberg, J. Appl. Phys. **34**, 1696 (1963). Numerous other references to polycrystalline line width are given in Ref. 12, p. 40.

[14] A. M. Clogston, H. Suhl, L. R. Walker, and P. W. Anderson, J. Phys. Chem. Solids **1**, 129 (1956).

[15] H. B. Callen and E. Pittelli, Phys. Rev. **119**, 1523 (1960).

existence of the two-magnon contribution to the line width in ferromagnetic insulators has been well studied experimentally[8,9,11,13] and theoretically.[10–12,14–16] The two-magnon contribution to the line shift has also been calculated for random pseudodipole coupling,[14] polycrystalline grain-to-grain variation in the anisotropy field[16] and surface pits, voids, and nonmagnetic inclusions.[7] In the Liu and Shaw experiments of I, nonmagnetic inclusions and voids are believed[17] to be responsible for the two-magnon process.

Four different types of experiments have been performed in which a linewidth originally controlled by two-magnon processes is reduced by operating under conditions which make the mode excited by the rf field lie outside the bulk magnon manifold. In the first type of experiment, Buffler[4] used values of applied field sufficiently low to make the uniform precession lie above the top of the bulk magnon manifold for spherical samples. His result of interest to us here is that for polycrystalline samples the linewidth reduces abruptly as the uniform precession passes above the top of the bulk magnon manifold. This is to be expected, since the two-magnon processes for scattering to low-wave-vector magnons are not possible when the uniform precession lies above the top of bulk magnon manifold. In the Buffler experiments there are Walker modes which lie above the top of the bulk magnon manifold, and there are spin wave modes degenerate with the uniform precession, even though these are separated from the uniform precession by rather large wave vectors. In the second type of experiment, White[5] and Nemarich[6] have measured the linewidth of magnetostatic modes which lie above the top of the bulk magnon manifold. The early experiment of White has not been explained, but Nemarich has interpreted his later experiment in terms of two-magnon scattering.

In the third type of experiment Risley and Bussey[2] varied the resonant frequency of the uniform precession by changing the angle that the sample, such as a rod-shaped one, makes with the applied field. Thus, they were able to continuously change the resonant frequency from above the top of the manifold to well within the manifold. Risley and Bussey[3] are presently making a thorough investigation of linewidths by this method, and there are preliminary indications that the results of our paper explain their experimental results quite well.

In the fourth type of experiment, which is of main interest here, Liu and Shaw[1] pumped the uniform precession below the bottom of the bulk magnon manifold in polycrystalline yttrium iron garnet. There are no magnetostatic modes or large-k modes degenerate with the uniform precession for the perfectly dense sample when the uniform precession is below the bottom of the bulk manifold. This was accomplished by using a disk-shaped sample with the applied dc field perpendicular to the plane of the disk so that the natural frequency of the uniform precession lies near the bottom of the bulk manifold. By using a polycrystalline sample with a large linewidth of 650 Oe (full linewidth) the uniform precession was driven with considerable amplitude (about one-half its resonant value) off resonance below the bottom of the bulk manifold.

In this way they found that the relaxation frequency of the uniform precession decreased from 650 Oe when the uniform precession was within the bulk manifold to about 150 Oe when the uniform precession was below the bottom of the bulk manifold. This reduction in the relaxation frequency has the obvious explanation that the two-magnon process is absent when operating below the bulk manifold.

There remains, then, the problem of explaining the large linewidth of the order of 150 Oe when the uniform precession is below the magnon manifold, since most presently known mechanisms[18,19] predict a linewidth of the order of 1 Oe. We propose that the 150-Oe relaxation frequency is indeed still dominated by the two-magnon relaxation to states which exist below the bulk dense magnon manifold by virtue of the modification of the manifold caused by the nonmagnetic inclusions in the samples. In Sec. II we discuss the nature of these modes and show how they provide an explanation of the experimentally observed large line widths outside the magnon manifold such as those of Liu and Shaw.

There are at least three other possible sources of the 150 Oe relaxation frequency. One is the effect of rare-earth impurities[20,21] which are known to cause large line broadening in impure yttrium iron garnet. The impurity content of the sample is unknown; however, an estimate of the impurities by J. M. Katz[22] based on known impurity concentration of other sample materials by the same supplier (Research Chemicals, Inc.) indicated that the rare-earth impurities are of the order of 0.01 weight percent, which is too low to explain the 150-Oe line width. Preliminary measurements by P. Wigen,[23] in which the linewidth changes from 550 to 610 Oe on going from room temperature to 77°K indicate (from the lack of the characteristic temperature peak of the impurity relaxation processes) that the 150 Oe is not due to an impurity relaxation process.

The second further source of loss is the three-magnon (in general, multimagnon) process induced by the nonmagnetic inclusions. In Sec. III we calculate the

[16] E. Schlömann, J. Phys. Chem. Solids **6**, 242 (1950).
[17] P. E. Seiden, C. F. Kooi, and J. M. Katz, J. Appl. Phys. **31**, 1291 (1960).
[18] T. Kasuya and R. C. LeCraw, Phys. Rev. Letters **6**, 223 (1961).
[19] P. Pincus, M. Sparks, and R. C. LeCraw, Phys. Rev. **124**, 1015 (1961).
[20] J. F. Dillon Jr., Phys. Rev. **127**, 1495 (1962).
[21] A more complete bibliography of the slowly and the rapidly relaxing impurity mechanisms is given in Secs. 6.2 and 6.3 of M. Sparks, *Ferromagnetic Relaxation Theory* (McGraw-Hill Book Company, Inc., New York, 1964).
[22] J. M. Katz (private communication).
[23] P. Wigen (private communication).

effect of this process and show that it provides a relaxation frequency about two orders of magnitude smaller than the experimental value.

Finally, the nonzero relaxation frequency of the magnons degenerate with the uniform precession[16] can give rise to a relaxation frequency outside the manifold, but this effect is too small to explain the observed linewidths; relaxation frequencies of the degenerate magnons which are typically two orders of magnitude larger than the relaxation frequencies measured by the parallel pumping experiments (see Ref. 12, p. 208) are required. This is discussed in Sec. IV.

In addition, we discuss briefly two more topics of significance to the theory of the magnon relaxation. In Sec. IV it is pointed out that the experimental result (Ref. 12, p. 208) that the degenerate magnon relaxation frequency is two orders of magnitude smaller than the uniform precession relaxation frequency is consistent with the present theory. Finally, in Sec. V the dependence of the linewidth on the applied field for fields such that the frequency is within the bulk manifold is discussed.

Agreement between the theory of the present paper and experimental results[1-4] is good although a detailed comparison is difficult (as discussed in Sec. II) since both η and δH are functions of the applied field H_{app}. The infinities in the relaxation frequency and line shift occurring at the top and bottom of the manifold in the previous theories[7,10,11,14-16] are removed and reasonable values of relaxation frequency and line shift are obtained by the manifold-broadening mechanism of Sec. II. This mechanism gives the correct order of magnitude of the relaxation frequency and linewidth both inside and outside the manifold.

II. RELAXATION FREQUENCY AND LINE SHIFT OUTSIDE THE SPIN-WAVE MANIFOLD

This section is concerned with an explanation of the relatively large relaxation frequencies observed[1-4] outside the manifold. In particular, we consider the 150-Oe uniform-precession relaxation frequency below the bottom of the spin-wave manifold observed in I. The theory of two-magnon relaxation previously has been based on the scattering of uniform precession magnons into states in the magnon manifold suitable for a perfectly dense sample. This explains the 650-Oe relaxation frequency when the uniform precession is within the spin-wave manifold. For frequencies below the bottom of the manifold, i.e., $\omega<\omega_i\equiv\gamma(H_{\text{app}}-4\pi N_z M_s)$, it is clear that the relaxation frequency of the two-magnon process is zero because there are no states into which the uniform precession can scatter with energy conservation. Therefore, it is not surprising that the relaxation frequency decreases strongly below the manifold. The value of 150 Oe below the manifold is quite large and is not explainable in this simple picture.

It is apparent, however, that the bulk manifold, that is, the manifold appropriate to a sample containing no pores, is not the correct one for a sample containing nonmagnetic pores and inclusions. In the vicinity of a pore the demagnetizing field of the pore causes the net field to differ from that expected in a perfectly dense sample. This means that the magnon manifold in the vicinity of the pore is different from that in the rest of the sample. Thus, the magnon manifold is modified by the pores in such a way that there are states below the bottom of the bulk manifold. The remaining 150-Oe relaxation frequency is then explained naturally in terms of two-magnon scattering into these degenerate modes. Our method is essentially to treat the diagonal terms in the quadratic part of the Hamiltonian as changing the dispersion relation and the off-diagonal terms as causing the scattering.

The modes below the bottom of the bulk band arise as follows: We assume that the mean free path of the magnons is short with respect to the pore size so that the demagnetization field of the pore varies little over a magnon mean free path. Since the mean free path in our sample is probably of the same order of magnitude as the pore size, the following explanation must be considered as a rough approximation, the actual condition lying between the short-mean-free-path case considered here and the long-mean-free-path case considered previously.[10-12] In this short-mean-free-path limit, each region around the pore may be considered as having its own dispersion relation. In the region near the top of a spherical pore, the z component of the demagnetization field will be $-4\pi N_z M_s$, with $N_z=\frac{2}{3}$, a factor of $\frac{2}{3}$ arising from the pore and a factor of 1 arising from the surface of the disk-shaped sample. Thus the magnons in this region can have energies below the bottom of the bulk band (since $N_z=1$ for the bulk band) as seen by the high-field approximation to the magnon dispersion relation[12]

$$\omega_k=D\hbar^{-1}k^2+\omega_a-N_z\omega_m+\tfrac{1}{2}\omega_m\sin^2\theta_k, \qquad (2.1)$$

where D is the exchange constant, k is the wave vector, ω_a is the applied field in frequency units, $\omega_m=4\pi\gamma M_s$, and θ_k is the angle between the applied field and the wave vector.

The relaxation frequency $1/T$ now can be calculated simply by using the new density of degenerate states in the Sparks, Loudon, and Kittel[10] two-magnon scattering result as modified by Seiden and Sparks[11]

$$1/T=2\pi^2\gamma M_s p G_{SS}, \qquad (2.2)$$

where

$$G_{SS}=0.109(3\cos^2\theta_u+1.4)^2/\cos\theta_u.$$

Here p, the porosity, is the total volume of all pores divided by the sample volume, and θ_u is the value of θ_k in (2.1) for $k=0$ and $\omega_k=\omega_u$, the uniform-precession frequency, i.e.,

$$\omega_u=\omega_a-N_z\omega_m+\tfrac{1}{2}\omega_m\sin^2\theta_u,$$

or

$$\cos\theta_u=[1-(2/\omega_m)(\omega_u-\omega_a+N_z\omega_m)]^{1/2}. \quad (2.3)$$

The factor 1.4 in G_{SS} of Eq. (2.2) unfortunately cannot be obtained from first principles,[11] and would be considered as an adjustable parameter. Rather than adjusting the parameter to fit the data, we choose a value (of 1.4 which was used in Ref. 11) in order to obtain a better test of the theory. The effect on the line width and line shift of choosing a different value of this parameter is discussed below. Equation (2.2) is to be replaced by $1/T=0$ when the uniform-precession frequency is outside of the manifold. With $4\pi M_s=1750$ Oe, $p=0.16$, and $\cos\theta_u=1$, this gives $\Delta H=1/\gamma T=850$ Oe, in fair agreement with the measured value of 650 Oe from I. The factor G_{SS} in (2.2) will vary from one region around the pore to another since N_z varies from region to region, thereby changing $\cos\theta_u$ according to (2.3). We must average $1/T$, or equivalently G_{SS}, over the sample of volume V

$$G=\frac{1}{V}\int_\Delta d\mathbf{r}\frac{0.109(3\cos^2\theta_u+1.4)^2}{\cos\theta_u}, \quad (2.4)$$

where $\cos\theta_u$ is given by (2.3) and Δ is the volume over which θ_u is within the manifold, i.e., over which $0<\cos^2\theta_u<1$.

The value of N_z in (2.3) as a function of the position $\mathbf{r}=(r,\theta,\varphi)$ of the elementary volume of integration in (2.4) for a spherical pore of radius R is

$$N_z=1+\tfrac{1}{3}(3\cos^2\theta-1)(R^3/r^3), \quad (2.5)$$

where the one comes from the surface of the disk-shaped sample and $(R^3/3r^3)(3\cos^2\theta-1)$ comes from the pore.

From (2.3) and (2.5) the integral (2.4) can now be written as

$$G=\frac{0.109}{V}\int_\Delta d\mathbf{r}\frac{\{3[1+\delta-\frac{2}{3}(3\cos^2\theta-1)R^3/r^3]+1.4\}^2}{[1+\delta-\frac{2}{3}(3\cos^2\theta-1)R^3/r^3]^{1/2}}, \quad (2.6)$$

where Δ is the volume for which $0<1+\delta-(2R^3/3r^3)\times(3\cos^2\theta-1)<1$, and δ is the distance of the uniform precession below the bottom of the bulk manifold in units of the width of the manifold, i.e.,

$$\omega_u=\omega_a-\omega_m-\delta\tfrac{1}{2}\omega_m,$$

or

$$\delta=2/\omega_m(\omega_a-\omega_m-\omega_u).$$

The volume of integration in (2.6), which contains N pores of radius R, is approximated by $\int d\mathbf{r}\cong N\int(\mathfrak{R}/R)\times dr\, r^2 4\pi\int_0^1 du$, where $u=\cos\theta$ and $(4\pi/3)\mathfrak{R}^3=V/N$. Then with $p=R^3/\mathfrak{R}^3$ and defining $z=r/R$, (2.6) becomes

$$G=3p(0.109)\int_1^{p^{-1/3}}dz\,z^2\int_{0_\Delta}^1 du \times\frac{\{3[1+\delta-\frac{2}{3}(3\cos^2\theta-1)(1/z^3)]+1.4\}^2}{1+\delta-\frac{2}{3}(3\cos^2\theta-1)(1/z^3)}. \quad (2.7)$$

Exact evaluation of the integral in (2.7) is difficult; however, we can extract the main features of G, that is, the cutoff value of ω_u below which G vanishes, the value of G for the uniform precession within the manifold, the value of G for the uniform precession just below the bottom of the bulk manifold, and the width of the region of applied fields over which G drops from its low field value (for the uniform precession within the bulk manifold) to its high field value (for the uniform precession just below the bottom of the bulk band). The cutoff value of the uniform-precession frequency ω_u below which the integral vanishes is obtained by examining the region in which $\cos\theta_u$ of (2.3) is between 0 and 1, i.e., where the uniform precession is within the manifold. For the maximum value of $N_z=1+(\frac{2}{3})$, (2.3) and $\cos^2\theta_u<1$ give

$$\omega_u>\omega_a-\omega_m-\tfrac{2}{3}\omega_m,$$

so the cutoff is $(\frac{2}{3})\omega_m\cong 1$ kOe below the bottom of the bulk manifold. This is in good agreement with the experimental observation that the relaxation frequency drops by a factor of approximately 1/2 in going from just below the bottom of the bulk manifold to 500 Oe below the bottom of the bulk manifold.

For the uniform precession within the bulk manifold, i.e., $-1<\delta<0$, G is very closely approximated for $p\ll 1$ by

$$G=0.109(3\cos^2\theta_{uB}+1.4)^2/\cos\theta_{uB} \quad \text{(inside manifold)}, \quad (2.8)$$

where $\cos\theta_{uB}=(1+\delta)^{1/2}$ is the value of $\cos\theta_u$ for the bulk manifold. So averaging G gives the bulk value of G_{SS} for the uniform precession within the bulk manifold for small porosity. This shows that within the bulk manifold our previous theory[10,11] is not seriously modified by the smearing of the spectrum due to the pores. The result (2.8) is almost obviously an examination of (2.7). Here Δ is very nearly the total region between R and $\mathfrak{R}$, and $\frac{2}{3}(3\cos^2\theta-1)R^3/r^3$ is negligible with respect to $1+\delta$ over almost all of this region.

For the uniform precession below the bottom of the bulk manifold, that is, for δ positive and of the order of 1, the somewhat tedious evaluation of the integral in (2.7) shows that G is of the order of the porosity p. The fact that $G\sim p$ is not surprising since it is the volume close to the pore which has a dispersion relation differing appreciably from the bulk value. Mathematically this results from $\Delta\cong$pore volume in (2.7). The ratio of $1/T$, or equivalently G, just above the bottom of the bulk manifold to that just below the bottom is of the order of $1/p=6.4$, in agreement with the experimental value of $650/150=4.3$.

The decrease from the high-field value of relaxation frequency to the low-field value occurs over a change of field of approximately $(R^3/\mathfrak{R}^3)4\pi M_s p$. For the sample in I this gives 250 Oe, which is compatible with the measurements of I.

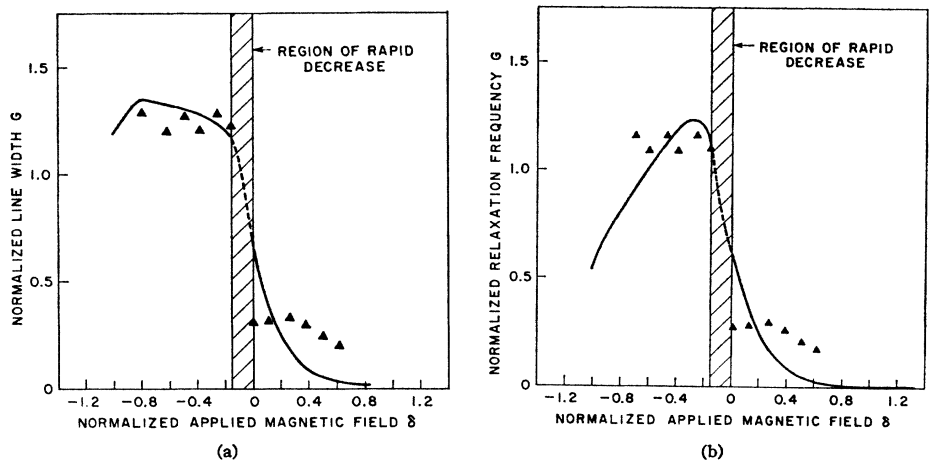

FIG. 1. (a) Comparison of calculated and experimental line widths below the bottom of the bulk manifold ($b=1.4$). (b) Comparison of calculated and experimental line widths below the bottom of the bulk manifold ($b=3$).

The above features are displayed explicitly in Figs. 1 and 2, which were obtained by machine evaluation of (2.7) for various values of porosity. The ordinate G is the line width divided by $2\pi^2\gamma M_s p$, and the abscissa is the applied magnetic field divided by $2\pi M_s$ with the zero shifted to the bottom of the bulk manifold. Figure 1 corresponds to a porosity of 0.16 for the sample in I. The "experimental points" of I, indicated by triangles, are normalized to $G=1.1$ within the manifold in Fig. 1(a). In Fig. 1(a) the value of the parameter b in (2.2) is $b=1.4$, while in Fig. 1(b) this value has been changed from 1.4 to 3, giving a more realistic shape of the relaxation frequency curve within the manifold. The "experimental points" were obtained from the χ'' curve by setting δH equal to a constant so that only the order of magnitude of these points and not the shape of the curve has meaning, as explained in the following paragraph.

Unfortunately, it is impossible to determine the values of relaxation frequency η and line shift δH from the single experimental curve of the imaginary part of the susceptibility χ'' as a function of frequency. This is because both η and δH are functions of frequency, so it is impossible to calculate both η and δH from the single χ'' curve using the "Lorentzian" expression

$$\chi''(H_{\rm app})=(\text{constant})\eta/[(H_{\rm app}-H_{\rm res}-\delta H)^2+\eta^2]. \quad (2.9)$$

The unshifted (Kittel) resonant frequency $H_{\rm res}$ is[12]

$$H_{\rm res}=\gamma^{-1}\omega+4\pi M_s N_T-4\pi M_s N_z \quad (2.10)$$

for a disk with the applied magnetic field perpendicular to the plane of the disk, where N_T and N_z are the transverse and z demagnetization factors, respectively. In these expressions, both η and δH are functions of the applied field $H_{\rm app}$. An order of magnitude of the experimental value of η can be obtained by setting the line shift δH equal to a constant independent of the applied field in Eq. (1.1) and solving this equation for η as a function of χ''. In this way an experimental curve of η as a function of the applied field is obtained, as in I. Points from this curve are reproduced as triangles in Fig. 1 herein. The order of magnitude of the value of η obtained in this way is correct, but the details of the curve must not be taken literally. For example, the relative flatness of the experimental triangle curve of Fig. 1 between $\delta=0$ and $\delta=0.6$ is definitely not correct and results from the approximation of setting δH equal to a constant. This can be seen by noticing that in solving the above expression of χ'' as a function for η, the resulting value of η will have a plus and minus type solution since this equation is quadratic in η.

Now, for the case of δH and η both constant, the plus solution for η must be chosen within the half-power points, and the minus solution for η must be chosen outside the half-power points. The plus and minus solutions cross at the half-power points and there is no problem. By setting δH equal to a constant in the χ'' curve of I the fundamental problem arises that the plus and minus solutions never cross. Within the manifold the plus solution is relatively constant giving a relaxation frequency of 650 Oe (in units of field). At the bottom of the manifold this plus solution increases very rapidly as the field is increased, in other words, as we go farther below the bottom of the manifold. Now, the minus solution for η is equal to zero at the maximum of the χ'' curve. This minus solution increases as the field is increased, goes through a maximum at a value of field corresponding to δ approximately equal to 0.3, as seen in Fig. 1, and then decreases. So the flatness of the experimental curve in Fig. 1 in the region $\delta=0$ to 0.6 results from the fact that this η minus curve goes to zero at the peak of the χ'' curve. There is, of course, no fundamental problem here; this difficulty arises from setting δH equal to a constant, which is not correct. The details of considering the correct behavior of χ'' when both η and δH are functions of the applied field are considered in Ref. 7.

So we see that we can extract the order of magnitude of η from the experiments, but we cannot obtain an accurate graph of η as a function of applied field because

δH is also a function of applied field. To obtain more than an order-of-magnitude comparison of theory and experiment, the values of η and δH are calculated theoretically and a graph of χ'' is drawn using Eq. (1.1). This theoretical χ'' curve is then compared directly with the experimental χ'' curve. This is much less satisfactory than a direct comparison of a calculated relaxation frequency with an experimental relaxation frequency at every value of applied field, but the χ'' comparison is the best that can be done.

It appears that if both the real and imaginary parts of the susceptibility were measured experimentally the expressions relating the susceptibility to the line shift and the relaxation frequency could then be solved for both the relaxation frequency and the linewidth as a function of frequency. The real and imaginary parts of the susceptibility are, of course, related by the Kramers-Kronig relations.

Figure 2, for $p=0.032$ and $p=0.001$, illustrates the sharpening of the transition region at the bottom of the manifold $\delta=0$ and the approach to (2.8) as p becomes small. They also indicate that G is of the order of p below the bottom of the bulk manifold. The general features of the theoretical results are in agreement with the experimental results as discussed above. The shape of the curve within the manifold is discussed in Sec. V. From Ref. 7 the expression for the line shift δH is given by

$$\delta H=-P\gamma^{-1}\sum_k \frac{[F(k)]^2}{\omega-\omega_k}, \qquad (2.11)$$

where P denotes principal part (of the integral corresponding to $\sum_k$), $F(k)$ is the coefficient of $a_0^\dagger a_k$ in the scattering Hamiltonian of (3.11), ω is the rf drive frequency, and ω_k is the frequency of spin wave k. This standard result of second-order perturbation theory is obtained formally from the usual line shape expression[10–12] by replacing $\delta(\omega-\omega_k)$ in $1/2T$ by $P[\pi(\omega-\omega_k)]^{-1}$. Evaluation[7] of the summation in (2.11) with $3\cos^2\theta_k-1$ in (3.11) replaced by $3\cos^2\theta_k+b$ as in Ref. 11, gives

$$\delta H=\tfrac{1}{2}[1/(b^2+3b+3)]p(4\pi M) \times[(3u_u^2+b)^2A_0-6b-3-9u_u^2], \qquad (2.12)$$

where

$$A_0\equiv(1/2u_u)\ln|(u_u+1)/(u_u-1)|.$$

We have defined u_u as

$$u_u=(1-\delta)^{1/2},$$

which is the value of the cosine of the angle between the spin-wave propagation vector and the applied field in the limit as the wave vector goes to zero and the energy of the magnon goes to the energy of the uniform-precession drive frequency (not the uniform-precession resonant frequency). Equation (2.12) is valid when the uniform precession is driven below the top of the spin-wave manifold (and also above the top of the manifold with u_u coupled). Evaluation[7] of the summation in (2.11) for the uniform precession above the bottom of the manifold gives a formally different result which we shall not need here. The result (2.12) should, of course, be averaged over the different demagnetization fields around a pore just as the relaxation frequency was. This will remove the narrow infinity at $u_u=1$. Investigation of the result (2.12) indicates that the line shift is relatively independent of the parameter b when the uniform precession is driven below the bottom of the manifold. However, within the manifold the line width δH is relatively sensitive to the value of b chosen. As explained above, the value of b will be chosen as 1.4. The graph of δH as a function of $\delta=1-u_u^2$ is given in Fig. 3. Taking $b=-1$ as in (3.11) for purely spherical pits, (2.12) indicates that δH does not change sign within the manifold. When the average is taken of the demagnetization field around a pore this is no longer true. According to (2.12) the line shift is always positive when the uniform precession is below the bottom of the manifold (for any value of b). Examination of (2.11) shows also that the line shift is always negative when the uniform precession is driven above the top of the manifold. This is just the frequency pushing of coupled oscillators.

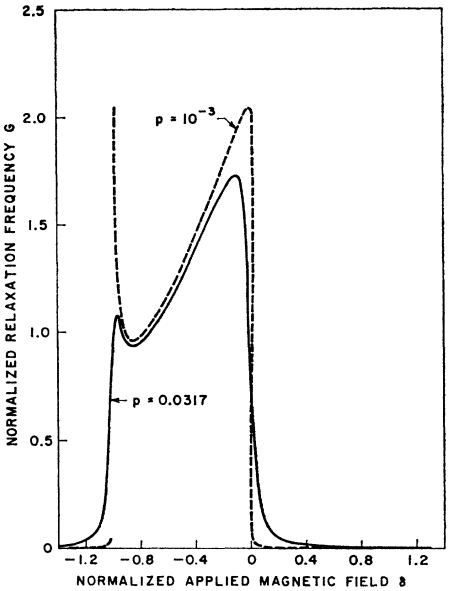

FIG. 2. Calculated linewidth for two small values of porosity.

We now want to calculate the χ'' curve using the relation (1.1) with the theoretical results (2.12) for δH and (2.2) and (2.7) for relaxation frequency η. The values of η are taken from Fig. 1(b), which was calculated from (2.7). The value of ηH which is used in (1.1) is obtained from (2.12), i.e., Fig. 3, by averaging this expression (2.12) over the demagnetization field around the pore as was done for η, which requires the evaluation of (2.12) above the top of the manifold and a rather involved machine calculation. Since the comparison of

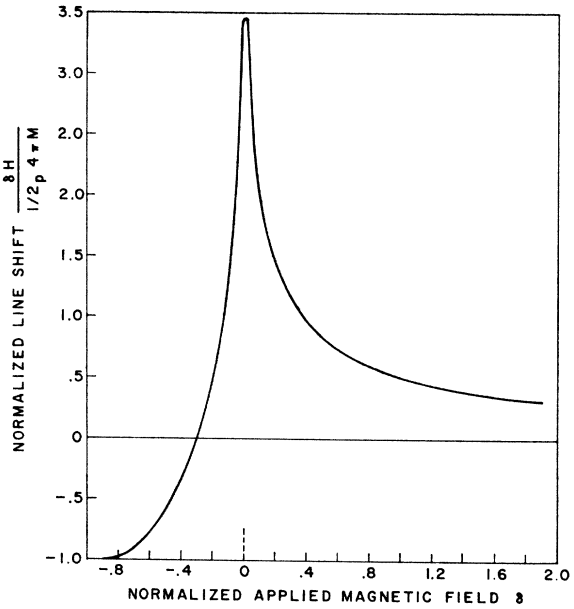

FIG. 3. Calculated line shift.

the theoretical χ'' curve with the experimental χ'' curve is not expected to be perfect, and since the value of δH within the manifold is relatively sensitive to the parameter b in (2.12) we make a simple approximation to δH of Fig. 3.

We can make a very good guess at the effect of averaging (2.12) over the demagnetization field of a pore. The main effect of averaging (2.12) is the removal of the infinity at $\delta=0$ and a lowering of the value of δH for values of δ slightly greater than -1. This lowering results from averaging in some of the large negative values of δH for δ slightly less than -1. Thus δH is equal to a finite constant at $\delta=D$ and drops off slowly as δ increases. The general shape of Fig. 3 within the bulk manifold ($-1<\delta<0$) is correct, with the slight lowering near $\delta=1$. Thus the approximation of Fig. 3 by the three straight-line segments

$$\begin{aligned}\delta H &= -205 \text{ Oe} \quad \text{for} \quad H_{\text{app}}<-205 \text{ Oe}\\ &= 2.47H_{\text{app}}+388 \quad \text{for} \quad -205 \text{ Oe}<H_{\text{app}}<274 \text{ Oe}\\ &= -0.47(H_{\text{app}}-835)+800 \quad \text{for} \quad 274 \text{ Oe}<H_{\text{app}}\end{aligned}$$

should be reasonably accurate. The amplitude of this curve was selected to make the width of the theoretical χ'' curve agree approximately with the width of the experimental χ'' curve. The value of this amplitude parameter is the correct order of magnitude predicted by the theory, but is probably somewhat higher than the value from the theory. This is somewhat ambiguous since the theory predicts an infinite δH at the bottom of the manifold. The general features of the theoretical χ'' are correct. The order of magnitude of the linewidth and the line shift are correct, and the general asymmetric shape is predicted by the theory. It should be emphasized that the porosity p and the nonspherosity factor b appearing in the expressions for η and ηH have been taken as fixed constants rather than treating these as parameters even though neither of these values are well known. By treating p and b as parameters, a much better agreement between theory and experiment could be obtained.

The resulting theoretical χ'', illustrated in Fig. 4, agrees quite well with the experimental points.

III. THREE-MAGNON UNIFORM-PRECESSION RELAXATION

In this section the contribution to the linewidth from three-magnon scattering of the uniform precession induced by the nonmagnetic pores in the sample is calculated. In order to calculate the scattering Hamiltonian, the model of a spherical cavity of radius R at the center of spherical sample of radius $r_0 (r_0 \gg R)$ is used. The magnetic potential at the position $\mathbf{r}$ is given by

$$\varphi(\mathbf{r})=-\int \frac{\operatorname{div}[\mathbf{M}(\mathbf{r}')\theta(r'-R)]}{|\mathbf{r}-\mathbf{r}'|}d\mathbf{r}', \tag{3.1}$$

where the function $\theta(r'-R)$ is 0 for $r'<R$ and 1 for $r'\geq R$, the origin of $\mathbf{r}$ and $\mathbf{r}'$ is the center of the cavity, and the integral extends over the sample. The demagnetization field of the cavity is the negative gradient of this potential. The magnetic moment $\mathbf{M}(\mathbf{r}')$ can be expanded in magnon creation and annihilation operators correct to third order as follows[12,24]:

$$\begin{aligned}M_z(\mathbf{r}')&=M_s-\frac{2\mu}{V}\sum_{\nu\mu}\exp[i(-\mathbf{k}_\nu+\mathbf{k}_\mu)\cdot\mathbf{r}']a_\nu^\dagger a_\mu,\\ M_x(\mathbf{r}')&=\frac{1}{2}\left(\frac{4\mu M_s}{V}\right)^{1/2}\sum_\nu[\exp(i\mathbf{k}_\nu\cdot\mathbf{r}')a_\nu+\text{c.c.}]\\ &\quad-\frac{1}{2}\left(\frac{4\mu M_s}{V}\right)^{1/2}\left(\frac{\mu}{2VM_s}\right)\\ &\quad\times\sum_{\lambda\mu\nu}\{\exp[i(-\mathbf{k}_\nu+\mathbf{k}_\mu+\mathbf{k}_\lambda)\cdot\mathbf{r}']a_\nu^\dagger a_\mu a_\lambda+\text{c.c.}\},\\ M_y(\mathbf{r}')&=\frac{1}{2i}\left(\frac{4\mu M_s}{V}\right)^{1/2}\sum_\nu[\exp(i\mathbf{k}_\nu\cdot\mathbf{r}')a_\nu-\text{c.c.}]\\ &\quad-\frac{1}{2i}\left(\frac{4\mu M_s}{V}\right)^{1/2}\left(\frac{\mu}{2VM_s}\right)\\ &\quad\times\sum_{\lambda\mu\nu}\{\exp[i(-\mathbf{k}_\nu+\mathbf{k}_\mu+\mathbf{k}_\lambda)\cdot\mathbf{r}']a_\nu^\dagger a_\mu a_\lambda-\text{c.c.}\},\end{aligned} \tag{3.2}$$

where a_ν and $a_\nu^\dagger$ represent creation and annihilation operators of spin wave k_ν, V is the sample volume, M_s is the saturation magnetization and μ is defined as $\frac{1}{2}g|\mu_B|$.

Using (3.2), the magnetic potential $\varphi(\mathbf{r})$ becomes

$$\varphi(\mathbf{r})=\varphi_A(\mathbf{r})+\varphi_B(\mathbf{r}), \tag{3.3}$$

[24] C. Kittel, *Quantum Theory of Solids* (John Wiley & Sons, Inc., New York, 1963).

where

$$\varphi_A(\mathbf{r})=-\int\Bigg[\Bigg\{M_s-\frac{2\mu}{V}\sum_{\nu\mu}\exp[i(-\mathbf{k}_\nu+\mathbf{k}_\mu)\cdot\mathbf{r}']a_\nu^\dagger a_\mu\Bigg\}\cos\theta+\Bigg(\tfrac{1}{2}\Big(\frac{4\mu M_s}{V}\Big)^{1/2}\sum_\nu[\exp(i\mathbf{k}_\nu\cdot\mathbf{r}')\exp(-i\varphi)a_\nu+\text{c.c.}]$$
$$-\tfrac{1}{2}\Big(\frac{4\mu M_s}{V}\Big)^{1/2}\frac{\mu}{2VM_s}\sum_{\lambda\mu\nu}\{\exp[i(-\mathbf{k}_\nu+\mathbf{k}_\mu+\mathbf{k}_\lambda)\cdot\mathbf{r}']\exp(-i\varphi)a_\nu^\dagger a_\mu a_\lambda+\text{c.c.}\}\Bigg)\sin\theta\Bigg]\frac{\cos\theta'\delta(r'-R)}{|\mathbf{r}-\mathbf{r}'|}d\mathbf{r}',$$

and

$$\varphi_B(\mathbf{r})=-\int\Bigg(-\frac{2\mu}{V}\sum(-k_\nu^z+k_\mu^z)\exp[i(-\mathbf{k}_\nu+\mathbf{k}_\mu)\cdot\mathbf{r}']a_\nu^\dagger a_\mu+\frac{i}{2}\Big(\frac{4\mu M_s}{V}\Big)^{1/2}\sum_\nu\{k_\nu^-\exp[i\mathbf{k}_\nu\cdot\mathbf{r}']a_\nu-\text{c.c.}\}$$
$$-\frac{i}{2}\Big(\frac{4\mu M_s}{V}\Big)^{1/2}\frac{\mu}{2VM_s}\sum_{\lambda\mu\nu}\{(-k_\nu^-+k_\mu^-+k_\lambda^-)\exp[i(-\mathbf{k}_\nu+\mathbf{k}_\mu+\mathbf{k}_\lambda)\cdot\mathbf{r}']a_\nu^\dagger a_\mu a_\lambda-\text{c.c.}\}\Bigg)\frac{\theta(r'-R)}{|\mathbf{r}-\mathbf{r}'|}d\mathbf{r}'.$$

The magnetic potential (3.3) consists of two parts. The first part φ_A is induced by the moments on the surface of the cavity. The second part φ_B is induced by the magnetic moment in the bulk material. We make the approximation that the spin-wave spectrum is unaffected by the presence of the pit. The magnetic field at $\mathbf{r}$ can be evaluated easily by $\mathbf{H}(\mathbf{r})=-\text{grad}\varphi(\mathbf{r})$. Then, the scattering Hamiltonian is the integral

$$\mathcal{H}=-\tfrac{1}{2}\int\mathbf{H}\cdot\mathbf{M}d\mathbf{r}.$$

First, we calculate the contribution of φ_B to the scattering Hamiltonian of the uniform-precession magnon. If the cavity is small compared with the total volume of a sample, we can use the following approximation:

$$\int\frac{\exp(i\mathbf{k}\cdot\mathbf{r}')}{|\mathbf{r}-\mathbf{r}'|}\theta(r'-R)d\mathbf{r}'=4\pi\frac{\exp(i\mathbf{k}\cdot\mathbf{r})}{k^2}.$$

Then, φ_B is

$$\varphi_B=-\frac{i}{2}\Big(\frac{4\mu M_s}{V}\Big)^{1/2}4\pi\Bigg\{\sum_\nu\frac{\exp(i\mathbf{k}_\nu\cdot\mathbf{r})}{k_\nu^2}k_\nu^-a_\nu-\sum_\nu\frac{\exp(-i\mathbf{k}_\nu\cdot\mathbf{r})}{k_\nu^2}k_\nu^+a_\nu^\dagger\Bigg\}$$
$$+i\Big(\frac{2\mu}{V}\Big)4\pi\sum_{\mu\nu}\frac{\exp[i(-\mathbf{k}_\nu+\mathbf{k}_\mu)\cdot\mathbf{r}]}{|-\mathbf{k}_\nu+\mathbf{k}_\mu|^2}(-k_\nu^z+k_\mu^z)a_\nu^\dagger a_\mu-\frac{i}{2}\Big(\frac{4\mu M_s}{V}\Big)^{1/2}\Big(\frac{\mu}{2VM_s}\Big)$$
$$\times4\pi\Bigg\{\sum_{\lambda\mu\nu}\frac{\exp[i(-\mathbf{k}_\nu+\mathbf{k}_\mu+\mathbf{k}_\lambda)\cdot\mathbf{r}]}{|-\mathbf{k}_\nu+\mathbf{k}_\mu+\mathbf{k}_\lambda|^2}(-k_\nu^-+k_\mu^-+k_\lambda^-)a_\nu^\dagger a_\mu a_\lambda-\text{c.c.}\Bigg\}.\quad(3.4)$$

Therefore, the scattering Hamiltonian of a uniform-precession magnon is

$$\mathcal{H}_B^{(2)}=8\pi^2R^3\Big(\frac{\mu M_s}{V}\Big)\sum_k(3\cos^2\theta_k-1)\Big[\frac{j_1(kR)}{kR}\Big](a_0^\dagger a_k+a_0a_k^\dagger),\quad(3.5)$$

$$\mathcal{H}_B^{(3)}=\xi\sum_{\mathbf{k}\mathbf{k}'}[F_B(kk')a_0a_ka_{k'}^\dagger+\text{c.c.}],\quad(3.6)$$

where

$$\xi=8\pi^2R^3(4\mu M_s/V)^{1/2}(\mu/V),\quad(3.7)$$

$$F_B(\mathbf{k},\mathbf{k}')=\Big(\frac{k^-k_z}{k^2}+\frac{k'^-k_z'}{k'^2}+\frac{3}{2}\frac{(-k'^-+k^-)(-k_z'+k_z)}{|-\mathbf{k}'+\mathbf{k}|}\Big)\frac{j_1(|\mathbf{k}-\mathbf{k}'|R)}{|\mathbf{k}-\mathbf{k}'|R},\quad(3.8)$$

and j_1 is the first spherical Bessel function.[25]

[25] L. I. Schiff, *Quantum Mechanics* (McGraw-Hill Book Company, Inc., New York, 1955), 2nd ed., p. 77; M. Sparks, *Magnetic and Electric Resonance and Relaxation*, edited by G. Smidt (North-Holland Publishing Company, New York, 1963).

Next, we calculate the scattering Hamiltonian corresponding to φ_A. If we neglect spin-wave terms having $k\neq 0$, φ_A is

$$\varphi_A=-(4\pi R^3/3)\{M_s(\cos/r^2)+\tfrac{1}{2}(4\pi M_s/V)^{1/2}[a_0\exp(-i\varphi)+a_0^\dagger\exp(i\varphi)](\sin\theta/r^2)\}. \tag{3.9}$$

This corresponds to the magnetic potential induced by the magnetic-dipole moment $(4\pi/3)R^3M_s$ placed at the center of a cavity. Hence, the contribution to the scattering Hamiltonian is

$$\mathcal{H}_A^{(2)}=-\pi R^3\left(\frac{\mu M_s}{V}\right)\sum_k\int\frac{3z^2-r^2}{r^5}[a_0a_k^\dagger\exp(-i\mathbf{k}\cdot\mathbf{r})+\text{c.c.}]d\mathbf{r}$$

$$\mathcal{H}_A^{(3)}=-\tfrac{3}{2}\pi R^3\left(\frac{4\mu M_s}{V}\right)^{1/2}\left(\frac{2\mu}{V}\right)\sum_{\mathbf{k},\mathbf{k}'}\int\left\{\frac{z(x-iy)}{r^5}\exp[i(-\mathbf{k}'+\mathbf{k})\cdot\mathbf{r}]a_0a_{k'}^\dagger+\text{c.c.}\right\}d\mathbf{r}. \tag{3.10}$$

After evaluating the integral, the two-magnon term is the same as (3.5) and the three-magnon term is given by (3.6) if $F_B(\mathbf{k},\mathbf{k}')$ is replaced by

$$\tfrac{3}{2}[(-k'^-+k^-)(-k_z'+k_z)/|-\mathbf{k}'+\mathbf{k}|][j_1(|-\mathbf{k}'+\mathbf{k}|R)/|-\mathbf{k}'+\mathbf{k}|R].$$

Therefore, the total scattering Hamiltonian of a uniform-precession magnon is

$$\mathcal{H}^{(2)}=16\pi^2R^3\left(\frac{\mu M_s}{V}\right)\sum_k(3\cos^2\theta_k-1)\left[\frac{j_1(kR)}{kR}\right](a_0^\dagger a_k+a_0a_k^\dagger), \tag{3.11}$$

$$\mathcal{H}^{(3)}=\xi\sum_{\mathbf{k},\mathbf{k}'}[F(\mathbf{k},\mathbf{k}')a_0a_ka_k^\dagger+\text{c.c.}], \tag{3.12}$$

where

$$F(\mathbf{k},\mathbf{k}')=\left[\frac{k^-k_z}{k^2}+\frac{k'^-k_z'}{k'^2}+3\frac{(-k'^-+k^-)(-k_z'+k_z)}{|-\mathbf{k}'+\mathbf{k}|^2}\right]\frac{j_1(|\mathbf{k}-\mathbf{k}'|R)}{|\mathbf{k}-\mathbf{k}'|R}, \tag{3.13}$$

and ξ is defined by (3.7).

The scattering Hamiltonian of a uniform-precession magnon by the three-magnon process is given by (3.12). We now calculate the relaxation frequency due to this three-magnon process. The kinetic equation of the number of uniform magnons n_0 is given by the well-known formula[21]

$$dn_0/dt=-(n_0-\bar{n}_0)/T_{20}, \tag{3.14}$$

where the bar denotes thermal equilibrium and the transverse relaxation time T_{20} is given by

$$(1/T_{20})=(2\pi/\hbar)\xi^2\sum_{\mathbf{k}\mathbf{k}'}|F(\mathbf{k},\mathbf{k}')|^2(n_k-n_{k'})\delta(\hbar\omega_u+\hbar\omega_k-\hbar\omega_{k'}), \tag{3.15}$$

where n_k is the number of magnons having wave vector $\mathbf{k}$; F is defined in (3.13) and ξ in (3.7). We use the ferromagnetic dispersion relation for spin waves,[12,14]

$$\omega_k=\gamma[(H_0-N_z(\omega_m/\gamma)+(D/\hbar\gamma)k^2)(H_0-N_z(\omega_m/\gamma)+(D/\hbar\gamma)k^2+4\pi M_s\sin^2\theta_k)]^{1/2}, \tag{3.16}$$

for k much smaller than the Brillouin-zone boundary value. For high fields, this is approximated by[12]

$$\omega_k=\omega_i+(D/\hbar)k^2, \tag{3.17}$$

where $\omega_i=\gamma H_0-N_z\omega_m$ and N_z is the z demagnetizing factor which has the value 1 for a disk-shaped sample with the applied field perpendicular to the plane of the disk. The energy of the uniform-precession magnon $\hbar\omega_u$ is very nearly equal to $\hbar\omega_i$ because $\hbar\omega_u$ is just below the top of the manifold of the spin-wave spectrum. We shall find that the important magnons have wave vectors too near the Brillouin-zone boundary for (3.16) or (3.17) to be valid; so a modification will be made below. The relaxation frequency for the three-magnon scattering is calculated for both dispersion relations (3.17) and the modified one (3.37).

Using (3.17), the δ function of (3.15) becomes

$$\delta(\hbar\omega_u+\hbar\omega_k-\hbar\omega_{k'})=\frac{1}{2D(\hbar\omega_u/D+k^2)^{1/2}}\delta[k'-(\hbar\omega_u/D+k^2)^{1/2}]. \tag{3.18}$$

Making the usual assumption that the $\mathbf{k}$ and $\mathbf{k}'$ magnons remain in thermal equilibrium, we have

$$n_k - n_{k'} = \frac{(\hbar\omega_u/k_BT)\exp((Dk^2+\hbar\omega_i)/k_BT)}{[\exp((\hbar\omega_i+Dk^2)/k_BT)-1][\exp((\hbar\omega_i+\hbar\omega_u+Dk^2)/k_BT)-1]}. \tag{3.19}$$

Here we used the approximation $\hbar\omega_u/k_BT \ll 1$, which is well satisfied for $\omega_u = 5\times 10^{10}$ sec^{-1} and room temperature. If we replace the summations over $\mathbf{k}$ and $\mathbf{k}'$ in (3.15) by integrals, $1/T_{20}$ is written as

$$\frac{1}{T_{20}} = \frac{2\pi}{\hbar}\xi^2\left(\frac{V}{8\pi^3}\right)^2 \int\int |F(\mathbf{k},\mathbf{k}')|^2 \frac{(\hbar\omega_u/k_BT)\exp((Dk^2+\hbar\omega_i)/k_BT)}{[\exp((\hbar\omega_i+Dk^2)/k_BT)-1][\exp((\hbar\omega_i+\hbar\omega_u+Dk^2)/k_BT)-1]} \times \frac{1}{2D(\hbar\omega_u/D+k^2)^{1/2}}\delta[k'-(\hbar\omega_u/D+k^2)^{1/2}]d\mathbf{k}d\mathbf{k}'. \tag{3.20}$$

The angular dependence of the integrals in (3.20), which is determined by bracket factor in $F(\mathbf{k},\mathbf{k}')$ as defined by (3.13), makes an exact evaluation of these integrals rather tedious. For an order-of-magnitude calculation this bracket angle factor can be replaced by a constant. Since an upper bound to the square of this factor is 25, we use the reasonable value of 10 so that (3.13) becomes

$$|F(\mathbf{k},\mathbf{k}')|^2 = 10[j_1(|\mathbf{k}-\mathbf{k}'|R)/(|\mathbf{k}-\mathbf{k}'|R)]^2. \tag{3.21}$$

The factor $j_1(|\mathbf{k}-\mathbf{k}')|R)/|\mathbf{k}-\mathbf{k}'|R$ of $F(\mathbf{k},\mathbf{k}')$ is an oscillating and decreasing function of $|\mathbf{k}-\mathbf{k}'|R$. In order to further simplify the calculation we approximate this function by

$$\begin{aligned} j_1(|\mathbf{k}-\mathbf{k}'|R)/|\mathbf{k}-\mathbf{k}'|R &= \tfrac{1}{3} \quad \text{for} \quad |\mathbf{k}-\mathbf{k}'|R \leq \gamma_1, \\ &= 0 \quad \text{for} \quad |\mathbf{k}-\mathbf{k}'|R \sim \gamma_1, \end{aligned} \tag{3.22}$$

where $\gamma_1 = 4.61$ is the first zero point of the spherical Bessel function j_1. This approximation means that only the spin waves which satisfy the condition $|\mathbf{k}-\mathbf{k}'|R \leq \gamma_1$ contribute to the relaxation of the uniform-precession magnon. This condition is rewritten as

$$u_{kk'} \geq \frac{[\hbar\omega_u/D-(\gamma_1/R)^2]+2k^2}{2k(\hbar\omega_u/D+k^2)^{1/2}} \equiv u_0, \tag{3.23}$$

where $u_{kk'}$ is the cosine of the angle between $\mathbf{k}$ and $\mathbf{k}'$. Thus (3.22) may be written

$$[j_1(|\mathbf{k}-\mathbf{k}'|R)/(|\mathbf{k}-\mathbf{k}'|R)]^2 \cong \tfrac{1}{9}\theta(u_{kk'}-u_0), \tag{3.24}$$

where the θ step function is defined by $\theta(x)=0$ for $x<0$ and 1 for $x>0$ and u_0 is defined in (3.23). In evaluating the integral over $d\mathbf{k}'$, we choose the z axis along $\mathbf{k}$ so that in (3.24) $u_{kk'}=u'$, where u' is the cosine of the angle between $\mathbf{k}'$ and the z axis. Then the azimuthal-angle integral gives 2π and the polar-angle integral becomes

$$\int_{-1}^{1} du'\theta(u'-u_0) \begin{cases} = 1-u_0 & \text{for} \quad u_0<1, \\ = 0 & \text{for} \quad u_0>1. \end{cases} \tag{3.25}$$

This condition $u_0<1$ determines the lower limit k_L of the k integral

$$k_L = [D^{-1}\hbar\omega_u - (\gamma_1/R)^2]/[2\gamma_1/R]. \tag{3.26}$$

On evaluating the two azimuthal angle integrals and the k' integral, (3.20) becomes

$$\frac{1}{T_{20}} = \frac{(2\pi)^3}{\hbar}\xi^2\left(\frac{V}{8\pi^3}\right)^2 \frac{10}{18D}\frac{\hbar\omega_u}{k_BT}\int_{k_L}^{k_m} k^2dk \int_{-1}^{1} du \int_{-1}^{1} du'\theta(u'-u_0) \times \frac{\exp((Dk^2+\hbar\omega_i)/k_BT)(\hbar\omega_u/D+k^2)^{1/2}}{[\exp((\hbar\omega_i+Dk^2)/k_BT)-1][\exp((\hbar\omega_i+\hbar\omega_u+Dk^2)/k_BT)-1]}, \tag{3.27}$$

where k_m defines the Brillouin-zone boundary in the spherical-boundary approximation. From (3.25) and (3.26) this reduces to

$$\frac{1}{T_{20}} = \frac{5\xi^2V^2\hbar\omega_u}{9\hbar Dk_BT}\int_{k_L}^{k_m} dk\, k\{2k[(\hbar\omega_u/D)+k^2]^{1/2} - [(\hbar\omega_u/D)-(\gamma_1/R)^2+2k^2]\} \times \frac{\exp[(Dk^2+\hbar\omega_i)/k_BT]}{\{\exp[(\hbar\omega_i+Dk^2)/k_BT]-1\}\{\exp[\hbar\omega_u+\hbar\omega_i+Dk^2)/k_BT]-1\}}. \tag{3.28}$$

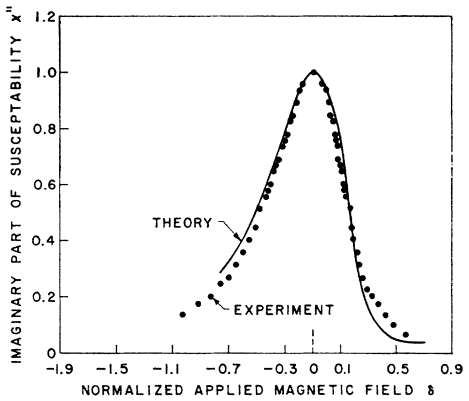

FIG. 4. Comparison of experimental (points) and theoretical (solid) line shape χ''.

This can be simplified by examining the relative sizes of the terms in the first brace $\{\ \}$: $\hbar\omega_i/D \cong \hbar\omega_u/D \cong 7\times10^{11}$ cm^{-2}; with[8] $R=4\times10^{-4}$ cm, $(\gamma_1/R)^2\cong10^8$ cm$^{-2}\ll\hbar\omega_u/D$. Thus, (4.13) reduces to

$$k_L\cong\hbar\omega_u R/2D\gamma_1\cong3.3\times10^7\text{cm}^{-1}, \tag{3.29}$$

so that

$$k_L^2\gg\hbar\omega_u/D\gg(\gamma_1/R). \tag{3.30}$$

With this inequality and

$$[(\hbar\omega_u/D)+k^2]^{1/2}\cong k+\hbar\omega_u/2Dk+(\hbar\omega_u)^2/8D^2k^3,$$

the brace factor reduces to

$$\{2k[(\hbar\omega_u/D)+k^2]^{1/2}-[(\hbar\omega_u/D)-(\gamma_1/R)^2+2k^2]\}\cong(\gamma_1/R)^2-(\hbar\omega_u/2Dk)^2. \tag{3.31}$$

The integral in (3.28) can now be evaluated numerically for any values of temperature and of ω_i and ω_u. It is more instructive to evaluate this integral by making the high-temperature approximation, which with (3.30) gives for (3.19)

$$n_k-n_{k'}\cong\hbar\omega_u k_BT/2D^2k^4. \tag{3.32}$$

A factor of $\frac{1}{2}$ is included as a correction because the high-temperature approximation is not very well satisfied, since $Dk_L^2/k_BT\cong2.5$ at 300°K. Using (3.31) and (3.32), (3.28) becomes

$$\frac{1}{T_{20}}=\frac{5\xi^2V^2\hbar\omega_u k_BT}{18\hbar D^3}\int_{k_L}^{k_m}dk\,k^{-3}\left[\left(\frac{\gamma_1}{R}\right)^2-\left(\frac{\hbar\omega_u}{2Dk}\right)^2\right].$$

The value of the integral is $D^2\gamma_1^4/(\hbar\omega_u)^2R^4$; with ξ^2 from (3.7) we have

$$1/T_{20}(3)=640\pi^4\gamma_1^4\mu^3M_sk_BTR^2/9DV\hbar^2\omega_u, \tag{3.33}$$

where (3) denotes three-magnon process.

The two-magnon linewidth is from Refs. 10 and 11 with $G(\theta_u)=0.109[(3\cos^2\theta_u-1)+2.4]^2/\cos\theta_u=2.1$ for our geometry, where θ_u is the angle between $\mathbf{k}$ and the applied field for a magnon having the frequency of the uniform precession and k approaching zero

$$1/T_{20}(2)=[(2.1)16\pi^3R^3\mu M_s]/3hV. \tag{3.34}$$

The factor 16 in Eq. (9) of Ref. 4 is incorrect and should read 32. Thus, with $\gamma_1=4.61$, we have

$$[1/T_{20}(3)]/[1/T_{20}(2)]=[10^3\mu^2k_BT]/[D\hbar\omega_uR]. \tag{3.35}$$

At 300°K and taking[17] $R=4\times10^{-4}$ cm this gives

$$[1/T_{20}(3)]/[1/T_{20}(2)]=10^{-2}. \tag{3.36}$$

This is an order of magnitude smaller than the observed value of $150/(650-150)=0.3$.

Now from (3.19) we see that k_L is not negligible with respect to the Brillouin-zone boundary wave vector so that the approximate dispersion relations (3.16) and (3.17) are not valid. The dispersion relation for yttrium iron garnet is not known, but the curve in Fig. 5 should not be a bad approximation. In this figure a construction is shown which gives k' as a function of k from the energy delta function $\delta(\hbar\omega_{k'}-\hbar\omega_k-\hbar\omega_u)$. In the expression (3.20) for $1/T_{20}$ the function $[j_1(|\mathbf{k}'-\mathbf{k}|R)/|\mathbf{k}'-\mathbf{k}|R]^2$, which decreases rapidly as $|\mathbf{k}'-\mathbf{k}|$ increases, is largest where $k'-k$ is small, i.e., in the linear region of Fig. 5. Thus the approximate linear dispersion relation

$$E_k=Ak, \tag{3.37}$$

where A is the order of E_m/k_m as defined in Fig. 5 should give order-of-magnitude accuracy in (3.20). It is not difficult to rework the above calculation using (3.37) in place of (3.17). In this case $|\mathbf{k}'-\mathbf{k}|R$ is always much larger than γ_1 so that (3.22) must be replaced by the asymptotic expression

$$[j_1(|\mathbf{k}'-\mathbf{k}|R)/|\mathbf{k}'-\mathbf{k}|R]^2\cong\cos^2(|\mathbf{k}'-\mathbf{k}|R)/|\mathbf{k}'-\mathbf{k}|^4R^4.$$

The rapidly oscillating cosine-squared function can be replaced by the average value $\frac{1}{2}$. In evaluating the resulting integral,

$$\frac{1}{T_{20}}=\frac{40\mu^3M_s\hbar\omega_uk_BTR^2}{\hbar VA^3}\int_0^{2\pi}d\varphi_k\int_{-1}^{1}du_k\int_0^{k_m}dk\times\frac{[k+(\hbar\omega_u/A)]^2}{|\mathbf{k}'-\mathbf{k}|^4}, \tag{3.38}$$

we approximate $|\mathbf{k}'-\mathbf{k}|^{-4}$ by $(k'-k)^{-4}=(A/\hbar\omega_u)^4$ within the solid angle $(\hbar\omega_u/Ak)^2$, i.e., where $|\mathbf{k}'-\mathbf{k}|\cong k'-k=\hbar\omega_u/A$, and zero outside this solid angle; this is valid for $k\geqq(\hbar\omega_u/A)$. For $k\leqq(\hbar\omega_u/A)$ we approximate $|\mathbf{k}'-\mathbf{k}|^{-4}$ by the same value of $(A/\hbar\omega_u)^4$, but within the total solid angle 4π. There results

$$1/T_{20}=[40\mu^3M_sk_mk_BTR^2]/[VA\hbar^2\omega_u]. \tag{3.39}$$

With $A=600k_B$ ergs/10^8 cm^{-1} this gives

$$[1/T_{20}(3)]/[1/T_{20}(2)]\cong10^{-4}.$$

Thus, using the more realistic dispersion relation (3.37) gives an even smaller result than (3.36). We conclude that the three-magnon scattering induced by the pores and nonmagnetic inclusions is too small to explain the observed[1-4] relaxation frequencies outisde the magnon manifold.

IV. RELAXATION FREQUENCY OF THE MAGNONS WHICH INTERACT WITH THE UNIFORM PRECESSION

The power-absorption line shape when the uniform precession is driven outside the manifold was explained in Sec. II in terms of the variation of the demagnetization field around a pore in the sample. An alternative explanation[16] is that the degenerate magnons with which the uniform precession interacts also have a finite relaxation frequency, as discussed in Sec. I. In the absence of these two effects the two-magnon theory predicts that the relaxation frequency η is identically zero outside the magnon manifold; thus, χ'' is identically zero outside the magnon manifold. There are other effects which can give rise to nonzero η outisde the magnon manifold, but all of these seem to be much smaller than the two effects we consider. For example, in evaluating the $\sum_k$ in the expression for η [which is obtained from Eq. (4.1) by replacing $P1/\pi(\omega-\omega_k)$ by $\delta(\omega-\omega_k)$], it is assumed[10] that the coupling coefficient $F(k)$ is strongly peaked at very small values of k. If this approximation is not made but the integral is evaluated exactly, then it is found that η is nonzero above the top of the manifold owing to the coupling of the uniform precession with the degenerate magnons which now have relatively large k vectors.

Parallel-pumping experiments indicate that the degenerate magnons relax much more slowly than the uniform precession, as discussed on p. 208 of Ref. 12. The reason[12] for the slower relaxation of the degenerate magnons is that their relaxation frequency is controlled by their long mean free path. This mean free path is in turn controlled by the spacing between the voids or nonmagnetic impurities. That is to say, the relaxing magnon is to be considered as a wave packet propagating through the sample; so it is not scattered by a given pit except when it comes near the pit. If the mean-free-path effect were not taken into account, the scattering calculation would predict that magnons having nonzero k would relax much more rapidly than uniform-precession magnons since the density of final states is proportional to k^2.

In order to illustrate explicitly the effect of introducing a relaxation frequency η_d for the degenerate magnons, we calculate the relaxation frequency $1/2T$ for the uniform precession for nonzero η_d in the present section. We find the not-too-surprising results that η_d must be approximately the same size as $1/2T$; in other words, in order to explain the experimental results,[1-4]

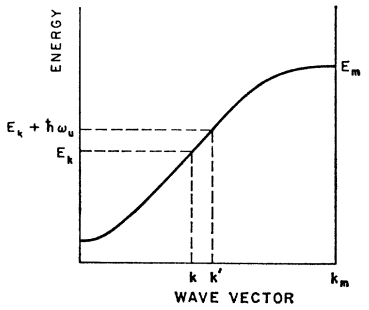

FIG. 5. Approximate magnon dispersion relation for yttrium iron garnet with a construction giving k' in (3.15) as a function of k from energy conservation.

the degenerate magnons must relax as fast as the uniform precession itself.

The usual expression [Eq. (7) of Ref. 10 before integrating over angles and with $(3\cos^2\theta_k-1)^2$ replaced by $0.109\ (3\cos^2\theta_k-1+2.4)^2\omega_u/\omega_i$ as discussed in Ref. 11] for the uniform-precession relaxation frequency

$$\frac{1}{T}=\frac{2\pi}{\hbar}\sum_k |F(\mathbf{k}R)|^2\delta(\hbar\omega_k-\hbar\omega_u), \tag{4.1}$$

where

$$F(\mathbf{k}R)=16(0.109)^{1/2}\pi^2R^3(\mu M_s/V)\times(3\cos^2\theta_k-1+2.4)(\omega_u/\omega_i)[j_1(kR)/kR]$$

is valid for strict conservation of energy, that is to say, for the limit of η_d going to zero. For nonzero lifetime η_d of the interacting $\mathbf{k}$ magnon the delta function must be replaced by a normalized Gaussian function:

$$\delta(\hbar\omega_k-\hbar\omega_u)\rightarrow(1/\pi\hbar)\eta/[(\omega_k-\omega_u)^2+\eta_d^2].$$

In the equation-of-motion derivation[7,14,16] the Gaussian arises directly, so the δ-function approximation is not made. Then, changing the summation to an integral $\sum_k=[V/(2\pi)^3]\int d\mathbf{k}$, evaluating the azimuthal angle as 2π, and evaluating the k integral by using the fact that $[j_1(kR)/kR]^2$ is large only for the small values of $k\lesssim R^{-1}$, and using $2\mu=\gamma\hbar$ and $\int_0^\infty d(kR)[j_1(kR)]^2=\pi/6$ gives

$$1/T_0(2)=[16\pi^3\mu M_sR^3J]/[3\hbar V]. \tag{4.2}$$

Here J is defined as

$$J=\frac{2}{\pi}\int_0^1 du\ 0.109(3u^2-1+2.4)^2\times\frac{\omega_u}{\omega_i}\frac{\eta_d\tfrac{1}{2}\omega_m}{\{[(\omega_i-\omega_u)/\tfrac{1}{2}\omega_m+1-u^2]^2+[\eta_d/\tfrac{1}{2}\omega_m]^2\}}, \tag{4.3}$$

where $u\equiv\cos\theta$. In the energy-conservation limit of $\eta_d/\tfrac{1}{2}\omega_m$ much smaller than one, this reduces to

$$J=[0.109(3\cos^2\theta_u-1+2.4)^2/\cos\theta_u]\omega_u/\omega_i \tag{4.4}$$

within the spin-wave manifold and zero outside the manifold, where

$$\cos^2\theta_u=(\omega_i-\omega_u)/\tfrac{1}{2}\omega_u+1,$$

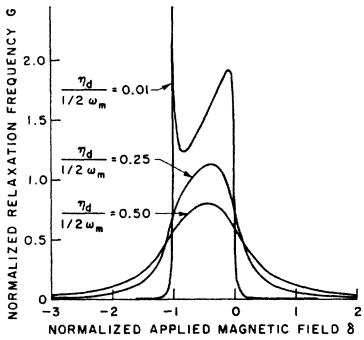

FIG. 6. Effect of relaxation frequency η_d of degenerate magnons on the uniform-precession relaxation frequency.

in agreement with the corrected Eq. (9) of Ref. 10. The factor 16 in Eq. (9) of Ref. 10 is incorrect and should be 32, and from Ref. 11 the factor $(3\cos^2\theta-1)^2$ is replaced by $0.109(3\cos^2\theta_u-1+2.4)^2(\omega_u/\omega_i)$. Here $\cos\theta_u$, the value of $\cos\theta_k$ in (3.16) with $\omega_k=\omega_u$, $k=0$ and $\cos\theta_k=\cos\theta_u$, is the value of $\cos\theta_k$ for the magnons into which the uniform precession scatters most strongly. The approximate dispersion relation

$$\omega_k=D\hbar^{-1}k^2+\omega_i+\tfrac{1}{2}\omega_m\sin^2\theta_k \tag{4.5}$$

has been used in obtaining (4.3). A compensating factor ω_u/ω_i is added to (4.3) to give the limiting result (4.4) in agreement with the result obtained from the correct dispersion relation (3.16). Here ω_i is defined for (3.17). This is the high-field approximation to (3.16) obtained by expanding the second factor in the square root. The two-magnon relaxation frequency $1/T_2$ is obtained by multiplying the single-pit result (4.2) by the number of pits $pV3/4\pi R^3$, where p is the fraction of the volume occupied by pits. With $\gamma\hbar=2\mu$ we have

$$1/\gamma T_2=2\pi^2M_s pJ, \tag{4.6}$$

with J defined by (4.3).

For arbitrary $\eta_d/\frac{1}{2}\omega_m$, on contemplating the integral $J(\omega_i-\omega_u)$ in (4.3), it becomes obvious that this function of $\cos^2\theta_u$ becomes very small as $(\omega_i-\omega_u)/\frac{1}{2}\omega_m$ becomes large and positive (i.e., for the uniform precession well below the bottom of the manifold) and drops to this small value in a width of $\omega_i-\omega_u$ of the order of η_d. In this limit $(\omega_i-\omega_u)/\frac{1}{2}\omega_m\gg1$, J reduces to the small value

$$J\cong\frac{8}{5\pi}\,\frac{\eta_d/\frac{1}{2}\omega_m}{[(\omega_i-\omega_u)/\frac{1}{2}\omega_m]^2+[\eta_d/\frac{1}{2}\omega_m]^2}.$$

The width $\eta_d/\frac{1}{2}\omega_m$ of the dropoff at $\omega_i=\omega_u$ of J as a function of $\omega_i-\omega_u$ is illustrated in Fig. 6 which was obtained by evaluating J numerically for the cases $\eta_d/\frac{1}{2}\omega_m=1/100$, $\frac{1}{4}$, and $\frac{1}{2}$. The linewidth is proportional to J according to (4.6). The abscissa is $\delta=1-u_u^2$, where $u_u^2\equiv\cos^2\theta_u\equiv1+[(\omega_i-\omega_u)/\frac{1}{2}\omega_m]$; this is linear in the applied field ω_0/γ since $\omega_i=\omega_0-4\pi\gamma M_s$. Notice that $\cos^2\theta_u=1$ corresponds to the crossing of the uniform precession below the bottom of the manifold and $\cos\theta_u=0$ corresponds to the top of the manifold. For the case $\eta_d/\frac{1}{2}\omega_m=1/100$ in Fig. 6, it is seen that the linewidth J drops sharply at $\cos^2\theta_u=1$ from $J=1.9$ to $J=0$. The width of the dropoff is $\Delta\cos^2\theta_u\cong1/50$ corresponding to $\Delta\omega_0/\gamma=(1/50)\frac{1}{2}\omega_m/\gamma=17.5$ Oe. For the case $\eta_d/\frac{1}{2}\omega_m=\frac{1}{4}$ the width of the dropoff at $\cos^2\theta=1$ is $\Delta\cos^2\theta_u\cong\frac{1}{2}$ corresponding to $\Delta\omega_0/\gamma=(\frac{1}{2})\frac{1}{2}\omega_m/\gamma=440$ Oe. These widths of $\Delta\cos^2\theta_u=1/50$ and $\frac{1}{2}$ for $\eta_d/\frac{1}{2}\omega_m=1/100$ and $\frac{1}{4}$, respectively, are both in agreement with the relation

$$\Delta\cos^2\theta_u=2\eta_d/\tfrac{1}{2}\omega_m, \tag{4.7}$$

which is equivalent to

$$\Delta\omega_u=2\eta_d. \tag{4.8}$$

Comparison of Fig. 6 with the "experimental" value of Fig. 5 from I indicates that the uniform-precession relaxation frequency $1/2T$ is of the correct order of magnitude for the value $\eta_d=0.25(\frac{1}{2})\omega_m=220$ Oe. This is two or three orders of magnitude larger than the usual parallel-pumping relaxation frequency. We conclude that the relaxation frequency of the degenerate magnons cannot explain the relaxation frequency of the uniform precession outside the manifold.

V. FIELD DEPENDENCE OF THE TWO-MAGNON LINEWIDTH

In this section the two-magnon linewidth for the uniform precession driven within the magnon manifold ($0\leqq\cos\theta_u\leqq1$ or $-1\leqq\delta\leq0$) is considered. The experimental low-field relaxation frequency from Fig. 6.3 of Ref. 1 indicates that the uniform-precession relaxation frequency is relatively independent of applied field over the full range $-1\leqq\delta\leqq0$ for which the uniform precession is excited within the magnon band.

The theoretical result (4.6) and the experimental curve from I are shown in Fig. 7. The theoretical curve of Fig. 7 is drawn for the energy-conservation limit $\eta_d/\frac{1}{2}\omega_m\to0$ so that J in (4.6) is given by (4.4). The agreement of the magnitude of the theoretical curve with the experimental curve is good in view of the crude mode used to derive the theoretical result (4.6). The strict field independence of the experimental results is

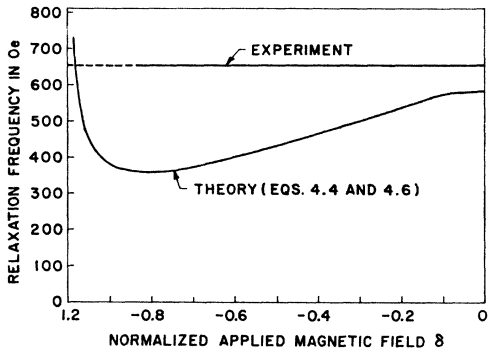

FIG. 7. Field dependence of uniform-precession relaxation frequency.

at first surprising, but it is possible that this is not in disagreement with the theory. As indicated in Ref. 11, the result (4.4) cannot be expected to give the exact functional dependence of the relaxation frequency on the applied field. It is interesting to note that if the constant factor 2.4 in (4.4), which was chosen to fit Seiden's[11] high-field data, is changed to 4, the relaxation frequency is constant to within 8% for $0.16 \leqq \cos^2\theta_u \leqq 1$ as shown in Fig. 8. Such a change in the constant seems not unreasonable since the "pores" in the present problem are nonmagnetic inclusion of a high density ($\Delta H = 650$ Oe), while the "pores" in Seiden's experiment are chiefly voids and surface pits of low density ($\Delta H \lesssim 50$ Oe). The shape of the pores may be different in the two cases and close spacing of pores destroys the spherical symmetry. The sharp rise in relaxation frequency at the top of the manifold ($\delta = -1$) in Figs. 7 or 8, which has been observed by Buffler,[4] was probably not observed by Liu and Shaw because $\delta = -1$ corresponds to the far tail of the Lorentzian curve, where the accuracy is very low. Also, as seen in Figs. 7 and 8, the increase in $1/T$ near $\delta = -1$ occurs at much smaller values of δ than for $1/T \sim 1/\cos\theta_u$, as predicted by Geschwind and Clogston.[26] Finally, the finite lifetime of the degenerate magnons (Sec. IV) and the modification of the dispersion relation by the pores (Sec. II) drastically reduce the peak at $\cos^2\theta_u = 0$.

As explained in Sec. II and Ref. 7, the line shift δH is equally as important as the relaxation frequency $1/T$ in determining the χ'' line shape. When the uniform-precession relaxation frequency $1/T$ is a constant, then the line shape is true Lorentzian if either δH is a constant or if δH is linear in the applied field. In the latter case of a linear δH, the linewidth of the χ'' curve is not given simply by $1/T$ but is determined by $1/T$ and the slope of the δH curve. It is quite reasonable that δH should be linear in the applied field over a large range of applied fields within the manifold. This observation has already been implicitly made in writing down the approximation to δH given under Eq. (2.10). We conclude that a true Lorentzian curve of χ'' within the magnon manifold is consistent with the theory.

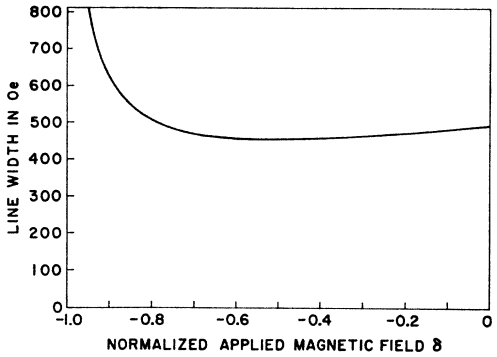

FIG. 8. Approximate applied field independence of uniform-precession relaxation frequency showing improved agreement of theory and experiment.

ACKNOWLEDGMENTS

Appreciation is expressed to P. Wigen for making the low-temperature measurement of Sec. I and to C. Kooi for furnishing information about the sample. We gratefully acknowledge several helpful conversations with S. H. Charap and H. J. Shaw. Appreciation is expressed to E. A. Tessman and C. Barry for the numerical computations. Appreciation is also expressed to A. S. Braun for his usual fine attention in supervising the typing of this report.

[26] S. Geschwind and A. M. Clogston, Phys. Rev. **108**, 49 (1957).